J. Phys. B: At. Mol. Phys. **18** (1985) 967-983. Printed in Great Britain

Electron–argon total cross section measurements at low energies by time-of-flight spectroscopy

J Ferch, B Granitza, C Masche and W Raith

Fakultät für Physik, Universität Bielefeld, D-4800 Bielefeld, Federal Republic of Germany

Received 14 May 1984, in final form 13 August 1984

Abstract. Recent improvements to our time-of-flight spectrometer are described in detail, in particular the redesign of the gas-target entrance and exit necessary for the essential elimination of a systematic error which affected the measurements near cross section minima. The modified spectrometer was used to measure the cross section of argon in the energy range of 0.08 to 20 eV. For the Ramsauer minimum of argon at 0.345 eV we obtain a cross section about twice as high as that of earlier experiments but in excellent agreement with another current experiment as well as with recent theoretical results and with cross sections derived from swarm experiments. At higher energies, our results agree well with other experimental and theoretical data.

1. Introduction

Since low-energy electron scattering is important for the understanding of weakly ionised plasmas (gas discharges, upper atmospheres of planets, interstellar clouds) great efforts have been made to improve the scattering theory by developing better methods of approximation and evaluating them in crucial comparisons with accurate experimental data. At low energies electron scattering from atoms and molecules is a rather complex interaction. In addition to the static Coulomb interaction, which dominates at higher energies and can be well described in the first Born approximation, there is a dynamic Coulomb interaction with the electric dipole moment of the atom induced by the scattered electron. Furthermore, spin exchange with the atomic electrons affects the interaction substantially.

Most desirable for comparisons with theory are differential cross section measurements on a single reaction channel. Total cross section measurements, on the other hand, offer experimental advantages which can be utilised to obtain more accurate data, especially at very low energies where differential experiments are extremely difficult because of limited intensity and energy resolution.

With decreasing energy total cross sections become more easily interpretable as the number of open channels and pertinent partial waves decrease. At zero energy the total cross section contains only s-wave scattering and equals the momentum transfer cross section determined in swarm experiments. For the extrapolation of measured cross sections to zero energy, the 'modified effective-range theory' (O'Malley 1963) provides useful formulae. The free-electron scattering at energies of a few meV is also of interest in assessing the scattering of atoms and molecules in high-n Rydberg states because the Rydberg electron behaves to a good approximation like a free electron of equal kinetic energy (Matsuzawa 1975).

0022-3700/85/050967+17$02.25

Experimental work on total cross sections for electron scattering from atoms and molecules started with the pioneer work of Ramsauer (1921, 1923), Brode (1925), Brüche (1927) and Ramsauer and Kollath (1929) in the 1920s. Bederson and Kieffer (1971) gave a comprehensive review of the state of art in this field. During the last decade both electron and positron total cross sections were measured by several groups up to energies of several hundred eV where the cross sections converge (Raith 1984).

Our time-of-flight (TOF) spectrometer has been developed from that of Land and Raith (1974) and was described in detail by Ferch *et al* (1980). In this paper we outline the principles of operation and discuss the modifications implemented recently. The capability of the improved spectrometer is demonstrated by the argon measurements reported here. Brief reports of this research have already been given (Ferch *et al* 1983a, b).

2. Description of the TOF spectrometer

Total cross sections are measured by determining the transmission of an electron beam through a gas target. Ideally, the simple relation

$$I(E) = I_0(E) \exp(-\sigma(E)nL) \tag{1}$$

applies, in which I_0 = primary electron beam intensity, I = transmitted intensity, E = electron energy, σ = total cross section, n = number density of target gas molecules, L = length of target.

The essential components of the spectrometer and its electronics are shown in figure 1. A 200 eV DC electron beam from a thermionic cathode is chopped in the

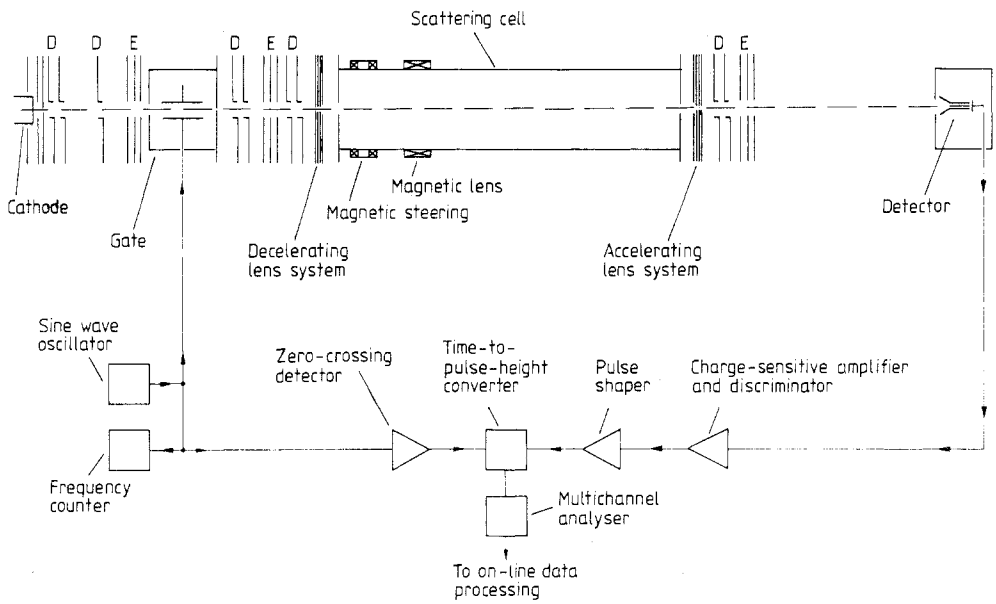

Figure 1. Layout of TOF spectrometer (not to scale) and electronics for data accumulation. D, deflector; E, einzel lens.

'gate' by sweeping it across a narrow slit of 0.1 mm width with a sinusoidal deflection voltage of 10–20 V (peak) and a frequency of typically 150–300 kHz. The time width of the resulting electron bursts is about 7 ns. The 200 eV electrons are decelerated before entering the target cell, the transmitted electrons are re-accelerated to 200 eV beyond the target exit and detected by a channel electron multiplier. During deceleration most electrons are defocused or even repelled. On the average less than one tenth of an electron per pulse reaches the detector. Along the beam path from cathode to detector several electrostatic einzel lenses are used for focusing and numerous beam deflectors for beam adjustment. The decelerating and accelerating systems also have focusing properties. In the low-energy target region only magnetic electron optical components, an einzel lens and two deflection coils are employed because electrostatic components would introduce undesired changes in kinetic energy. This weak magnetic lens (which has approximately the field distribution of a single current loop with a diameter of about one tenth the target length and a centre field strength of 0.3 to 3 G depending on the energy interval studied) is adjusted to get the optimum primary-beam transmission. That means, for a certain electron velocity it images the entrance onto the exit aperture but for other electron velocities within the broad distribution focusing is impaired by chromatic aberration. The lens also focuses electrons which undergo small-angle scattering while they are still near the entrance. This lens action reduces the forward scattering discrimination. On the other hand, the lens increases the transmitted primary-beam intensity by several orders of magnitude which is essential for the feasibility of the measurements.

For each detected electron the flight time is determined individually by measuring the time between detection and the following zero transition of the gate voltage (inverted timing). Flight-time measurements accumulated for up to 30 min form a flight-time distribution spectrum. Such spectra are measured with and without gas in the target. The intensity attenuation due to the gas usually lies between 1 : 3 and 1 : 10. By applying equation (1) for any given flight time one obtains the total cross section as a function of the flight time which can easily be converted into the kinetic energy of the electrons in the target region. Note that for each electron which reaches the detector at the end of the flight path its kinetic energy is determined individually from the TOF measurement. Therefore, the energy resolution is determined by timing accuracy and other effects discussed below but it is independent of the energy distribution of the primary electron beam. The latter limits only the energy range which can be covered in one TOF measurement. The thermionic electrons have an energy spread of about 0.6 eV. For measurements at very low energies the primary energy (or flight time) spectrum is far from flat because of the focusing properties of the beam transport system. It is already a stringent test of the spectrometer performance if pronounced structures in the spectrum $I_0(t)$, obtained without gas, do not lead to false structures in the cross section $\sigma(t)$. This is demonstrated in figure 2.

The layout of the vacuum and gas handling system is given in figure 3. Both cathode and detector region are separately pumped in order to reduce performance changes due to the influence of the target gas. Between gas target and main chamber a pressure ratio of about 100 is maintained. The target pressure is measured in a chamber connected to the target cell by a separate pipe. This manometer chamber houses a Baratron capacitance manometer and an MKS spinning rotor gauge used for absolute pressure measurements in different but overlapping ranges. For accurate determination of the target gas density from the measured pressure the temperature has to be known. Therefore, the temperature is monitored by platinum resistance thermometers at several

Figure 2. Example of a TOF measurement, here with CO_2. (*a*) Time distribution $I_0(t)$ of the electrons detected without target gas by means of 'inverted timing'. The left and right wings of the spectrum correspond to electron energies of 0.07 and 0.5 eV, respectively. Note the pronounced structure in the initial distribution $I_0(t)$. (*b*) Time distribution $I(t)$ obtained with target gas. (*c*) Distribution of $\ln(I_0/I)$, a quantity which is proportional to the total cross section $\sigma(t)$. Note that the structure of $I_0(t)$ does not lead to false structures in $\sigma(t)$.

positions. The capacitance manometer is temperature stabilised no more than 5° above target (room) temperature to minimise the effect of thermal transpiration.

For the general treatment of TOF spectroscopy we refer to the literature (Raith 1976). Although the basic principle of a TOF cross section measurement is simple, the following complications arise.

(i) The computation of the kinetic energy from the measured flight time is easy if one assumes that the energy changes from 200 eV to low energy and vice versa occur abruptly at well defined axial positions. However, since the deceleration and acceleration fields have axial extensions of several mm, a correction is required as described at the end of § 3.2.

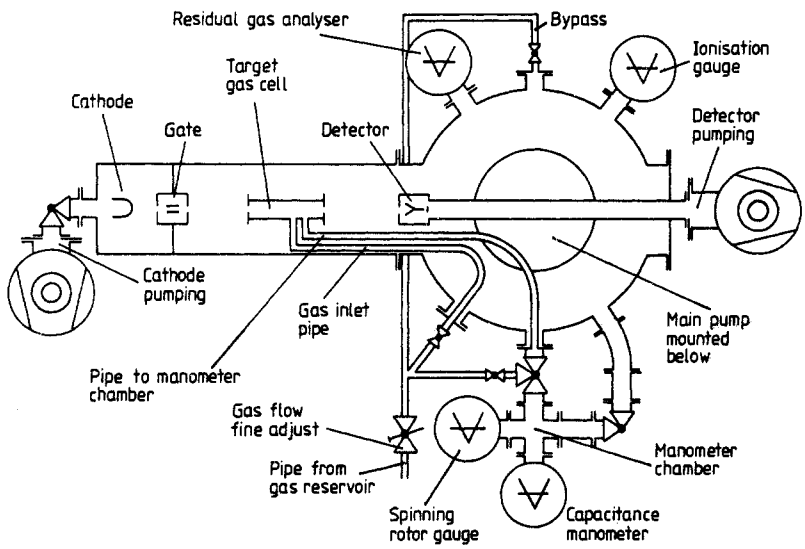

Figure 3. Layout of vacuum and gas-handling system. All three pumps are turbomolecular pumps. In order to ensure cleanliness the system can be baked at 200 °C for several days. The residual gas pressure in front of the target-gas inlet is of the order of 10 nTorr. The ionisation gauge which measures the background pressure in the main chamber can be calibrated (for each target gas separately) and then used as a convenient secondary manometer because the stationary-state background pressure is proportional to the target pressure.

(ii) The product nL in equation (1) is really a density integral along the axis. Its accurate determination is described in § 3.1.

(iii) The change of mode with/without gas in the target cell must not alter conditions outside the target. Electron optical properties, for example, can depend on gas pressure (work function changes due to gas layers on electrodes, pressure-related space charges due to trapped ions). In order to ensure that the gas pressure remains constant outside the target the gas flux is not turned off but rather bypassed. In the mode 'without gas' the same flux enters the main system.

(iv) For measuring $\sigma(E)$ over a wider energy range than covered by the thermionic electron beam, several TOF measurements, performed with different primary distributions, must be spliced together. In order to change the covered energy interval different potentials for target cell and adjacent electron optical components must be selected. The consistency of data from measurements with greatly different electron optical parameters ascertains that the splicing of data sets is not affected by systematic errors.

Our final cross section results are presented in form of a smooth $\sigma(E)$ curve (supplemented by tabulated values for selected energies). The raw data consist of numerous flight-time distribution measurements which yield cross section data for small energy intervals. The result of each measurement is entered into a plot extending over the whole energy range studied. Data taking is continued until each energy of the range is covered by several measurements, typically ten. At a selected energy the cross section value used for the $\sigma(E)$ curve is obtained by averaging the results of the individual measurements. This evaluation is made for as many selected energies as necessary for a unique $\sigma(E)$ determination.

The experimental error of the cross section measurements is obtained in the following way: (i) The error describing all uncorrelated fluctuations is computed from the variance of the different measurements at selected energies and amount to several per cent (table 1). (ii) The systematic error common to all $\sigma(E)$ values is estimated by analysing its sources, such a manometer calibration and target length determination. This error is smaller than 1%.

The resolvable energy, ΔE, of a TOF spectrometer depends on several sources of error with different dependence on the electron energy, E (Raith 1976). From design and performance parameters of our spectrometer we estimated the resolvable energy as

$$\Delta E(E) = 0.002 + 0.002E^{1/2} + 0.01E + 0.03E^{3/2} \tag{2}$$

where ΔE and E are given in eV. The first term is a conservative estimate for the error due to energy variations in the target, the second term describes the negligible Doppler broadening for a room temperature argon target, the third term is an upper limit for errors due to trajectory length variation of the electrons focused by the magnetic lens, and the fourth term represents the error due to timing uncertainty which dominates at higher energies. According to equation (2) ΔE varies from 0.003 to 2.9 eV over the covered energy range of $0.08 \leqslant E \leqslant 20$ eV; some intermediate values are $\Delta E = 0.01$, 0.03, 0.1, 0.5 and 1.0 eV for $E = 0.3$, 0.75, 1.9, 6.0 and 10.0 eV, respectively. Experimental data on narrow cross section structures, which could serve to demonstrate the actually achieved energy resolution at low energies, are not yet available. The measurements of the $e^- - O_2$ resonances (Land and Raith 1973, Ferch *et al* 1980) give only upper limits for ΔE because the resolved doublet peaks, separated by 0.02 eV, consist of bands of lines, each line corresponding to vibrational excitations from a different rotational level of the ground state.

Table 1. Measured total cross sections.

E (eV)	σ (10^{-16} cm^2)	$\pm\Delta\sigma/\sigma$(%)	E (eV)	σ (10^{-16} cm^2)	$\pm\Delta\sigma/\sigma$(%)
0.08	1.50	1.4	0.90	1.05	2.2
0.09	1.36	1.8	0.95	1.14	2.3
0.10	1.19	1.9	1.00	1.22	1.8
0.11	1.10	2.1	1.10	1.40	2.1
0.12	1.00	1.8	1.20	1.57	2.9
0.13	0.91	1.8	1.30	1.79	2.0
0.14	0.82	1.5	1.40	1.98	2.6
0.15	0.750	1.7	1.50	2.13	1.0
0.16	0.687	2.6	1.60	2.33	0.6
0.17	0.625	2.2	1.70	2.52	1.1
0.20	0.491	3.0	1.90	2.88	0.7
0.25	0.383	2.8			
0.30	0.327	2.4	2.0	2.97	1.3
0.345	0.311	2.6	3.0	4.84	2.5
0.40	0.328	2.5	4.0	6.45	2.7
0.45	0.367	1.9	5.0	8.64	1.7
0.50	0.416	2.6	6.0	10.1	0.6
0.55	0.478	1.6	7.0	12.1	1.1
0.60	0.548	1.7	8.0	14.0	0.9
0.65	0.624	1.7	10.0	18.9	0.2
0.70	0.70	1.5	12.0	23.1	0.6
0.75	0.78	1.7	14.0	24.0	0.9
0.80	0.87	1.9	16.0	23.5	0.5
0.85	0.96	2.0	20.0	20.2	0.8

The resolvable energy, ΔE, is the minimum separation required for resolving two unknown structures of $\sigma(E)$. That must not be confused with the uncertainty of assigning an energy E_i to a measurement of a cross section for which linearity of $\sigma(E)$ over the interval ΔE centred at E_i can be assumed. The latter is estimated for our spectrometer as ± 0.004 eV up to $E = 0.4$ eV and about $\pm 1\%$ of E at higher energies.

3. Spectrometer studies

3.1. Computation of target density distributions

The pressure in the manometer chamber is equal to the pressure in the target cell at the location where the connecting pipe is attached, provided that there is no unknown flow in that pipe due to leaks or getter action in the manometer chamber. However, inside the target cell there is a pressure variation ranging from the maximum at the feed-pipe connection to about half that pressure at both orifices and a gradual decrease to zero outside of the target. For the proper data evaluation the product nL of equation (1) has to be replaced by

$$n_m L_G = \int n(z, r=0)\,\mathrm{d}z \tag{3}$$

where n_m is the molecule density measured in the manometer chamber, L_G is the effective gas-cell length and $n(z)$ is the density distribution along the axis.

The density distribution can be computed on the basis of the following idealising assumptions.

(i) Stationary state of gas flow.

(ii) Molecule-wall collision treated as absorption followed by re-emission with an angular intensity distribution given by Lambert's law.

(iii) Free pathlength large compared with cell extensions.

(iv) Gas input from feed-pipe end also described by Lambert's law.

Density computations of this kind were reported by Mathur *et al* (1975). By following the ideas of these authors we developed our own formulae, enlarging the scope of the computation by including points away from the axis. Figure 4 shows a computed axial density distribution. The 'normalised density distribution' n^* is set to unity at the 'pressure gauge exit', that is, where the pipe leading to the manometer chamber is connected. At the gas inlet n^* reaches the maximum of 1.04. The function n^* decreases going axially to either end of the target cell. With the exception of the feed-pipe and orifice region, the radial density gradient is negligibly small. Qualitatively, the local density depends mostly on the solid angle under which both orifices are seen since these are the directions from which no molecules are emitted whereas all the directions pointing to inside walls of the target cell are those from which molecules are emitted with nearly equal intensity (along the wall n^* varies by no more than a few per cent). The extension of the gas distribution to the outside region of the orifice is shown in figure 5.

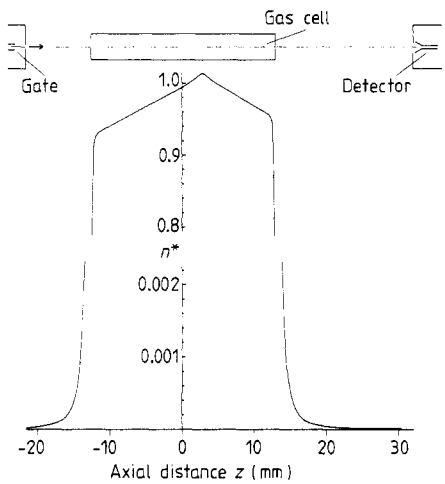

Figure 4. Profile of the normalised axial density distribution in the target cell computed for entrance and exit orifices of 1 mm diameter.

A crucial point of all transmission experiments for total cross section measurements is the discrimination against forward scattering. The 'cut off' solid angle, Ω_c, within which small-angle scattered electrons can still be transmitted to the detector should be as small as possible. An assessment of the resulting systematic error is complicated because Ω_c varies along the target axis. Averaging over the whole target length gives $\langle\Omega_c\rangle$ which is a meaningful result for isotropic (s wave) scattering. In order to estimate the error due to insufficient forward scattering discrimination for cases of anisotropic scattering, some knowledge of the angular dependence of the differential scattering is

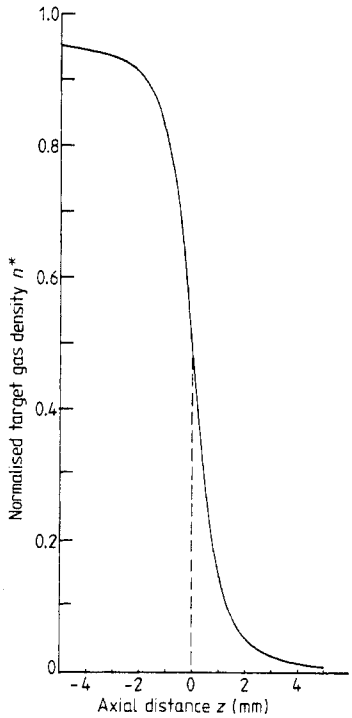

Figure 5. Axial density distribution function in the vicinity of the exit orifice.

required. At the lower energies covered in this experiment it suffices to consider the average cut-off solid angle $\langle\Omega_c\rangle$ for s-wave scattering and the forward scattering enhancement factor $f=(\mathrm{d}\sigma/\mathrm{d}\Omega)_{\theta=0}/(\sigma_{\text{total}}/4\pi)$, assuming that the differential cross section is approximately constant within Ω_c in forward direction.

By computing the cone defined by the exit orifice for each point on the axis we get $\Omega_c(z)$. By multiplying it with the local n^* value and integrating along the axis we obtain the averaged cut-off solid angle as $\langle\Omega_c\rangle=2.4\times10^{-4}$ sr. The magnetic lens increases the average cut-off solid angle because electrons which undergo small-angle scattering while near the target entrance are also focused. (However, this lens does *not* act like a longitudinal magnetic guiding field which could trap scattered electrons in helical trajectories.) Approximate calculations on the effect of the magnetic lens lead to the higher value of $\langle\Omega_c\rangle=1.5\times10^{-3}$ sr, corresponding to 1.2×10^{-4} of the sphere. Thus for s waves the undiscriminated forward scattering is completely negligible compared with the other cross section errors which typically amount to several per cent. Only if forward scattering were enhanced by a factor of 100 or more would its influence exceed the 1% level.

3.2. Modification of target design

The incentive for studying the possible systematic errors resulting from the target design was provided by our first measurements of the e-Ar total cross section at the Ramsauer minimum which gave values three times as high as known from the modern literature (Golden and Bandel 1966, Gus'kov *et al* 1978). In our target used up to

that time the gas cell and the region at target potential were identical. Thus, the deceleration (re-acceleration) occurred where the target gas emerged from the gas cell entrance (exit) orifice. The resulting scattering outside the gas cell can cause a substantial systematic error in cases where the cross section increases rapidly with energy. Our earlier measurements with this spectrometer (Ferch *et al* 1980, 1981, 1982) did not fall into this category and, therefore, were not affected by the effect considered here. Figure 6 illustrates the influence of the target design on measurements at the Ramsauer minimum of argon. Figure 6(a) shows the conditions for the old design. The proper drift region, in which the electrons have a constant low energy, starts well inside the gas cell at $z = +6$ mm as indicated by the flat portion of the $\sigma(z)$ curve on the right-hand side. As demonstrated in figure 6(b) this problem can be solved by a separation of the deceleration and re-acceleration region from the gas-cell entrance and exit, respectively. Now the proper drift region starts outside the gas cell at $z = -5$ mm. The details of the new target-end design are shown in figure 7.

After implementation of the new design our measured cross section values were lower but not yet consistent with the literature values. Our computations indicated that this systematic error had been eliminated completely and a further separation of the deceleration (re-acceleration) region and target entrance (exit) would not further change the results. Nevertheless, we checked this experimentally by performing additional measurements with the separation extended to 18 mm. The data did not change (figure 8).

With this new target design we have to distinguish between the 'effective gas-cell length' L_G which enters in equation (1) and the 'effective drift-tube length' L_D which is used in the conversion of measured flight time to kinetic energy. From the calculated target density distribution and equation (3) we obtained a value of $L_G = 24.7$ cm while the geometric separation of entrance and exit orifice is $L = 25.4$ cm. The determination of L_D is more difficult because it depends on the final energy in the drift tube and, to a smaller extent, on the intermediate potentials used in the deceleration and re-acceleration regions. From computations of the electric potential distributions and trajectory calculations with the program developed by Herrmannsfeldt (1965) we determined the flight times for various conditions. As a workable approximation we make a straightforward conversion of flight time to kinetic energy by assuming abrupt changes in energy at either end of a drift region of length L_D. This computation is then refined by a correction to the kinetic energy scale of a few meV. The drift length L_D, chosen for minimisation of the additional corrections, is 27.1 cm. This is somewhat shorter than the distance between the first and last electrode at gas-cell potential which is 27.4 cm in the new design.

4. Argon cross sections

The argon total cross section varies by nearly two orders of magnitude from a maximum at 14 eV to the Ramsauer minimum at 0.345 eV. At the Ramsauer minimum s-wave scattering vanishes. The remaining higher-order scattering amplitudes result in a strongly enhanced forward scattering which can lead to an error due to insufficient discrimination of small-angle scattering. From an estimate based on theoretical results for differential scattering (McEachran and Stauffer 1983) we conclude that the differential scattering in the forward direction is enhanced by the factor $f \simeq 20$ compared with

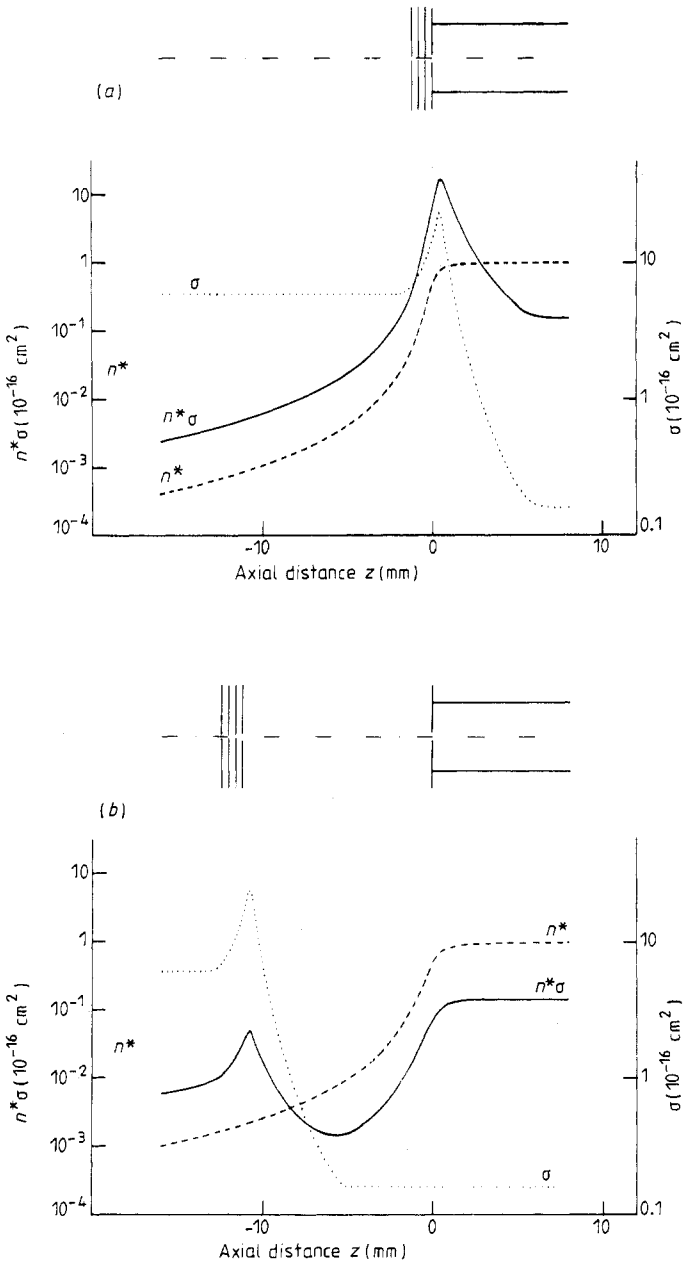

Figure 6. Example of scattering outside the target entrance. (*a*) Shown above the diagram is the target entrance (at $z = 0$) with the closely packed deceleration electrodes. The following functions are plotted: $n^*(z)$, the normalised gas density distribution (as in figure 4); $\sigma(z)$, the argon scattering cross section for the actual energy of the electrons at those axial positions, derived from the computed potential distributions for this electrode configuration; $n^*(z)\sigma(z)$, the product function which shows directly where most of the unwanted scattering takes place. (*b*) Same for a target design in which the deceleration occurs about 1 cm in front of the gas cell entrance. The peak of the unwanted scattering is reduced by more than a factor of 100.

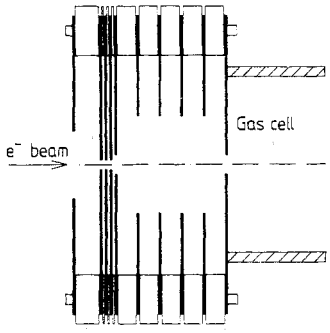

Figure 7. New design of target ends (here entrance). An extension package was inserted consisting of five copper spacers (each 2 mm thick) which give openings for differential pumping on all sides, four molybdenum plates (0.254 mm thick and having a 10 mm diameter centre hole) and a new gas cell entrance plate also made of molybdenum (with a 2 mm orifice diameter).

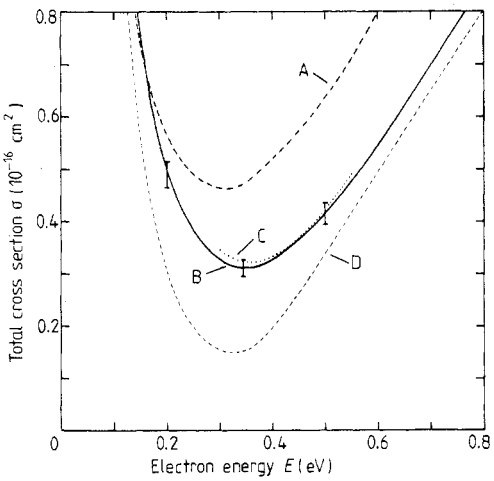

Figure 8. Measurements in the vicinity of the argon Ramsauer minimum. The data obtained with the old design (curve A) lie considerably above the results of Golden and Bandel (1966) and Gus'kov *et al* (1978) indicated by curve D. The data obtained with the new design (curve B) lie below curve A but still above curve D. A test with increased separation in the target-end design (curve C) did not lead to a further lowering of the minimum cross section.

s-wave scattering of equal total cross section. With $\langle\Omega_c\rangle/4\pi = 1.2\times10^{-4}$ and an enhancement factor of 20 we get an error of less than 0.3% for undiscriminated forward scattering at the Ramsauer minimum. This is only a small fraction of the uncertainty of the cross section measurement.

Because of the large variation of the cross section, the target gas pressure had to be varied accordingly in order to achieve sufficient attenuation of the beam at the selected energies. This required absolute pressure measurements over a wide range. We repeatedly checked that the measured cross sections are independent of gas pressure in order to prove the absence of pressure-related systematic errors.

The measured cross sections and their statistical errors are listed in table 1. In the energy range from 0.08 to 1.9 eV our data were obtained from overlapping TOF spectra. Above 1.9 eV the TOF spectra taken for cross section measurements at selected electron energies were too narrow for overlap. The listed statistical errors (one standard deviation) are all smaller than ±3% ; the systematic error common to all data is smaller than ±1%. The Ramsauer minimum was determined separately by fitting a third-order polynomial in energy to each spectrum containing it. By means of this procedure we located the Ramsauer minimum at $E_R = (0.345 \pm 0.005)$ eV. At higher energies, the TOF spectrometer is inferior to other spectrometers with regards to energy resolution. Nevertheless we extended our measurements up to 20 eV in order to cover the Ar cross section maximum and to get sufficient overlap with other experimental data.

Our results are plotted in figure 9 for comparison with other data. Independent of us, the group of Jost *et al* (1983) at the University of Münster obtained rather similar results with an entirely different experimental method. Both new results show a higher minimum cross section than obtained by Golden and Bandel (1966) and Gus'kov *et al* (1978). Obviously, the discrepancy indicates that unknown or underestimated systematic errors afflicted either the new or the preceding experiments. Systematic error analysis requires detailed information about an experiment. We cannot re-evaluate the errors of the preceding experiments. In general we think that insufficiently discriminated forward scattering is most likely the reason if a transmission experiment yields cross sections below the true values. The possibility of large-angle scattered electrons escaping from the target and reaching the detector via wall collisions (which would lead to a systematic error of the same sign) was tested and found to be completely

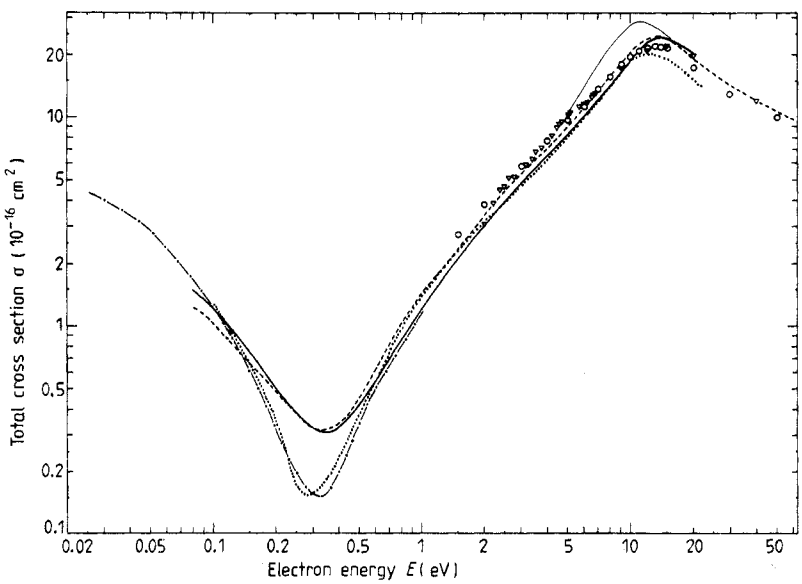

Figure 9. Our results compared with those of other groups. For clarity the theoretical results of Fon *et al* (1983), extending from 3 to 18 eV, were not included because they coincide, as do the results of McEachran and Stauffer below 5 eV, with the experimental data points. ——, this work; ——, McEachran and Stauffer (1983); - - -, Jost *et al* (1983); –·–·–, Gus'kov *et al* (1978); ·····, Golden and Bandel (1966); ○, Kauppila *et al* (1977); ▽, Charlton *et al* (1980).

negligible for our target arrangement (Ferch *et al* 1980); it is probably negligible for the other transmission experiments as well.

At higher energies additional data from Kauppila *et al* (1977) and Charlton *et al* (1980) are available. Both groups measured the electron total cross sections mainly for the purpose of direct comparison with their positron data. The agreement of all the plotted results in the 1 to 20 eV range is satisfactory. A cross section maximum about 10% higher (not shown in figure 9) was measured by Aberth *et al* (1964) in a crossed-beam experiment involving detection of scattered as well as unscattered atoms. The recent theoretical results of McEachran and Stauffer (1983), obtained with an adiabatic exchange approximation, are plotted in figure 9 only at higher energies where they deviate from the experimental results. Below 5 eV their results lie very close to the experimental data (for $E < 0.5$ eV see figure 11). The theoretical results of Fon *et al* (1983), obtained with the *R*-matrix method, were not plotted in figure 9 because they coincide with our curve at the cross section maximum and with the data points of Kauppila *et al* and Charlton *et al* at lower energies.

In our comparison with other experimental data we did not include all the old experiments which produced widely differing results and were technologically superseded by the work of Golden and Bandel (1966). However, it should be pointed out that the very first measurements, performed by Ramsauer (1921, 1923), Brüche (1927), and Ramsauer and Kollath (1929) withstood the test of time marvelously. The new results confirm what was measured 60 years ago. For a comparison of all the old data we refer to Gaertner (1931).

In order to compare the total cross sections, $\sigma(E)$, measured in beam experiments with the momentum-transfer cross sections, $\sigma_M(E)$, derived from swarm experiments, the modified effective-range theory (MERT) provides extrapolation formulae. Here we used the four-parameter MERT formulae which Haddad and O'Malley (1982) employed for evaluating the swarm data of Milloy and Crompton (1977) and Robertson (1977):

$$\sigma(E) = (4\pi/k^2) \sum_{L=0}^{\infty} (2L+1) \sin^2 \eta_L \tag{4}$$

$$\sigma_M(E) = (4\pi/k^2) \sum_{L=0}^{\infty} (L+1) \sin^2(\eta_L - \eta_{L+1}) \tag{5}$$

$$\tan \eta_0 = -Ak[1 + (4\alpha/3a_0)k^2 \ln(ka_0)] - (\pi\alpha/3a_0)k^2 + Dk^3 + Fk^4 \tag{6}$$

$$\tan \eta_1 = (\pi/15a_0)\alpha k^2 - A_1 k^3 \tag{7}$$

$$\tan \eta_L = \pi\alpha k^2/[(2L+3)(2L+1)(2L-1)a_0] \tag{8}$$

where k is the wavenumber (in atomic units) related to the energy E (in eV) by $E = 13.605\ (ka_0)^2$; a_0 is the Bohr radius. For equations (4)-(8) the approximation $\sin \eta \simeq \tan \eta$ applies. The free parameters to be determined by the fit are A, A_1, D and F. Scientifically most interesting is A, the scattering length related to the zero-energy cross section by $\sigma(0) = 4\pi A^2$. In equation (7) we used the parameter A_1 introduced by O'Malley (1963) rather than the related ε_1 of Haddad and O'Malley. For the dipole polarisability of argon we inserted the experimental value $\alpha = 11.08\ a_0^3$ (Reinsch and Meyer 1976). We employed the method for linearised regression described by Guest (1961). By trying summations of up to 100 phaseshifts we found that summing up to $L = 20$ was sufficient.

As input of the fitting procedure we used low-energy data points (σ_i, E_i) for selected energies up to an energy E_{max} together with their errors $\Delta\sigma_i$ and ΔE_i. We executed the fitting program for different values of E_{max} ranging from 0.2 to 2.0 eV. The experimental data points and the curves for four E_{max} values are shown in figure 10. If equations (4) and (6)–(8) were a good analytic form for describing the argon total cross section, the curves resulting from a MERT fit of data points up to E_{max} would continue close to the data points beyond E_{max}. However, as figure 10 illustrates the curves depart rather sharply from the data points at energies not far beyond E_{max}. Another indication for the limitations of the four-parameter MERT fit is the fact that the deviations of the fitted data points from the curve are not statistically distributed. This can be seen directly in figure 10 for $E_{max} = 1.5$ eV; for the other fits it is less obvious in the plot but clearly documented in the computer output. Below our lowest-energy data point at $E = 0.08$ eV the curves obtained with different E_{max} almost coincide. Nevertheless, the extrapolated zero-energy cross section, $\sigma(0)$, shows a systematic increase with increasing E_{max}. For $E_{max} = 0.3$, 0.5, 1.0 and 1.5 eV we get $\sigma(0) = (7.13 \pm 0.28)$, (7.39 ± 0.13), (7.64 ± 0.06) and $(7.93 \pm 0.05) \times 10^{-16}$ cm^2, respectively. The decrease of the statistical errors of the four fitting parameters with increasing

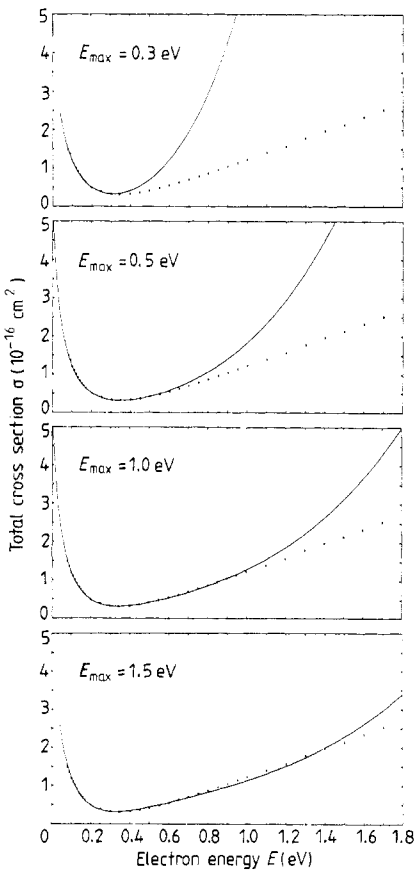

Figure 10. Selected data points and the curves given by the MERT formula fitted to the low-energy points up to $E_{max} = 0.3$, 0.5, 1.0 and 1.5 eV, respectively.

E_{max} is a consequence of the increasing data base. It should not be mistaken as a figure of merit for the goodness of the MERT fit. Since the main purpose of the MERT evaluation here is not the analytical description of the measured cross sections but rather the extrapolation to energies below the range of measurement, it follows that E_{max} should be chosen as low as compatible with the competing aim of getting sufficiently small statistical errors. For our case we concluded that $E_{max} = 0.4$ or 0.5 eV is the best choice and selected 0.5 eV, the lowest E_{max} for which Haddad and O'Malley (1982) reported parameter values (right-hand column, table 2). The left-hand column of table 2 shows our fit parameters with their correlated statistical errors. As our final result for the scattering length we quote $A = -(1.45 \pm 0.02)\, a_0$ which corresponds to $\sigma(0) = (7.4 \pm 0.2) \times 10^{-16}$ cm^2.

The presently available information on $\sigma(E)$ from $E = 0.5$ eV down to zero energy is summarised in figure 11. The agreement between the MERT curves obtained from

Table 2. Results of data fitting to MERT formulae with $E_{max} = 0.5$ eV.

Parameter	This work	Haddad and O'Malley (1982)
A/a_0	$-1.449 + 0.013$	-1.492
A_1/a_0^3	$8.50 + 0.07$	9.104
D/a_0^3	$73.1 + 2.1$	64.3
F/a_0^4	$-115.8 + 11.9$	-77.3

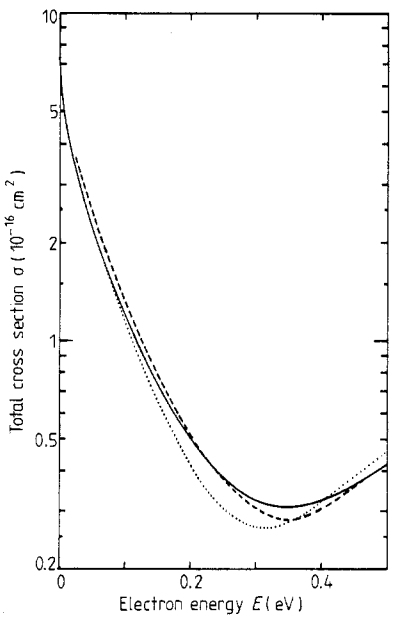

Figure 11. Argon total cross section below 0.5 eV obtained from MERT evaluation of beam data (——, this work) and swarm data (·····, Haddad and O'Malley 1982) and from a theory (– – –, McEachran and Stauffer 1983) based on the adiabatic exchange approximation. The zero-energy cross sections for the beam data and the swarm data MERT curves are 7.4 and 7.8×10^{-16} cm^2, respectively; theory yields 7.98×10^{-16} cm^2.

beam and swarm data is not perfect but adequate in view of the difficulties in extracting the information about $\sigma_M(E)$ from swarm data. Additional information can be expected from the MERT evaluation of the total cross section measurements of Jost *et al* (1983) and the low energy differential scattering data of Weyhreter *et al* (1984). The theoretical curve of McEachran and Stauffer (1983) is in very satisfactory agreement with the MERT results.

5. Conclusion

Argon has often been used as a calibration gas for cross section measurements. With its pronounced Ramsauer minimum it is even more interesting theoretically and experimentally than helium. The discrepancy between beam and swarm results which existed for many years was intolerable in view of the high experimental standards achieved by both techniques. The agreement reached now is very satisfactory. Our results also demonstrate that the TOF spectrometry has been developed into a reliable method for determining total cross sections. Its realm will always lie at the very lowest energies.

Acknowledgments

The early measurements which lead to the redesign of the target were performed in collaboration with Ms Sigrid Höwelmann. The authors thank Dr Jost and collaborators (University of Münster) for permitting the display of their data prior to final publication. This work has been supported by the University of Bielefeld and the Ministry for Science and Research of the State of Nordrhein-Westfalen.

Note added in proof. Directly related to our paper is the recently published work of K L Bell, N S Scott and M A Lennon 1984 *J. Phys. B: At. Mol. Phys.* **17** 4757-65. These authors employed an *R*-matrix approach and obtained results in good agreement with McEachran and Stauffer (1983) and, therefore, also in good agreement with the experimental results presented here.

References

Aberth W H, Sunshine G and Bederson B 1964 *Atomic Collision Processes* ed M R C McDowell (Amsterdam: North-Holland) pp 53-8

Bederson B and Kieffer L J 1971 *Rev. Mod. Phys.* **43** 601-40

Brode R B 1925 *Phys. Rev.* **25** 636-44

Brüche E 1927 *Ann. Phys., Lpz.* **84** 279-91

Charlton M, Griffith T C, Heyland G R and Twomey T R 1980 *J. Phys. B: At. Mol. Phys.* **13** L239-44

Ferch J, Granitza B and Masche C 1983a *Verhandl. DPG (VI)* **18** 229

Ferch J, Masche C and Raith W 1981 *J. Phys. B: At. Mol. Phys.* **14** L97-100

—— 1983b *Proc. 13th Int. Conf. on Physics of Electronic and Atomic Collisions, Berlin* ed J Eichler *et al* (Amsterdam: North-Holland) Abstracts p 90

Ferch J, Raith W and Schröder K 1980 *J. Phys. B: At. Mol. Phys.* **13** 1481-90

—— 1982 *J. Phys. B: At. Mol. Phys.* **15** L175-8

Fon W C, Berrington K A, Burke P G and Hibbert A 1983 *J. Phys. B: At. Mol. Phys.* **16** 307-21

Gaertner H 1931 *Ann. Phys., Lpz.* **8** 135-62

Golden D E and Bandel H W 1966 *Phys. Rev.* **149** 58-9

Guest P G 1961 *Numerical Methods of Curve Fitting* (Cambridge: Cambridge University Press) pp 336 ff, 366 ff

Gus'kov Yu K, Savvov R V and Slobodyanyuk V A 1978 *Sov. Phys.-Tech. Phys.* **23** 167–71
Haddad G N and O'Malley T F 1982 *Aust. J. Phys.* **35** 35–9
Herrmannsfeldt W B 1965 *SLAC Report* No 51
Jost K, Bisling P G F, Eschen F, Felsmann M and Walther L 1983 *Proc. 13th Int. Conf. on Physics of Electronic and Atomic Collisions, Berlin* ed J Eichler *et al* (Amsterdam: North-Holland) Abstracts p 91
Kauppila W E, Stein T S, Jesion G, Dababneh M S and Pol V 1977 *Rev. Sci. Instrum.* **48** 822–8
Land J E and Raith W 1973 *Phys. Rev. Lett.* **30** 193–5
—— 1974 *Phys. Rev.* A **9** 1592–602
Mathur B P, Field J E and Colgate S O 1975 *Phys. Rev.* A **11** 830–3
Matsuzawa M 1975 *J. Phys. B: At. Mol. Phys.* **8** L382–6
Milloy H B and Crompton R W 1977 *Aust. J. Phys.* **30** 51–60
McEachran R P and Stauffer A D 1983 *J. Phys. B: At. Mol. Phys.* **16** 4023–38 and private communication
O'Malley T F 1963 *Phys. Rev.* **130** 1020–9
Raith W 1976 *Adv. At. Mol. Phys.* **12** 281–373
—— 1984 *Proc. NATO Advanced Study Group on Positron Scattering in Gases* (London: Plenum) in print
Ramsauer C 1921 *Ann. Phys., Lpz.* **66** 546–58
—— 1923 *Ann. Phys., Lpz.* **72** 345–52
Ramsauer C and Kollath R 1929 *Ann. Phys., Lpz.* **3** 536–64
Reinsch E A and Meyer W 1976 *Phys. Rev.* A **14** 915–8
Robertson A G 1977 *Aust. J. Phys.* **30** 39–49
Weyhreter M, Barzick B and Linder F 1984 *Electronic and Atomic Collisions* ed J Eichler, I V Hertel and N Stolterfoht (Amsterdam: Elsevier) pp 547–52